Semiclassical analysis of the weak-coupling limit of SU(2) lattice gauge theory: The subspace of constant fields

J. Bartels
II. Institut für Theoretische Physik, Universität Hamburg, Hamburg, West Germany

T. T. Wu
CERN, Geneva, Switzerland and Gordon McKay Laboratory, Harvard University, Cambridge, Massachusetts 02138

(Received 9 November 1987)

This paper contains the first part of a systematic semiclassical analysis of the weak-coupling limit of lattice gauge theories, using the Hamiltonian formulation. The model consists of an N^3 cubic lattice of pure SU(2) Yang-Mills theory, and in this first part we limit ourselves to the subspace of constant field configurations. We investigate the flow of classical trajectories, with a particular emphasis on the existence and location of caustics. There the ground-state wave function is expected to peak. It is found that regions densely filled with caustics are very close to the origin, i.e., in the domain of weak field configurations. This strongly supports the expectation that caustics are essential for quantities of physical interest.

I. INTRODUCTION

In a previous paper[1] we proposed to perform a systematic investigation of the weak-coupling limit of non-Abelian lattice gauge theories with the help of the semiclassical approximation. In a formal sense the weak-coupling limit $g^2 \to 0$ of the lattice Hamiltonian[2]

$$H = \frac{g^2}{2} T + \frac{2}{g^2} V \tag{1.1}$$

(the electric part T is a second-order differential operator, the magnetic part V plays the role of the potential) is analogous to the $\hbar \to 0$ limit of the Schrödinger Hamiltonian in ordinary quantum mechanics. This suggests using a suitable generalization of the WKB approximation for investigating the $g^2 \to 0$ limit of (1.1). One is thus led to study classical nonlinear Hamiltonian systems with a larger number of variables.

There is overwhelming evidence that the classical Yang-Mills equations are not integrable.[3] One therefore has to face the possibility that many aspects of modern nonlinear mechanics and their relation to the semiclassical approximation of quantum-mechanical systems will play an important role.[4] One of the peculiarities that one encounters even in very simple non-Abelian lattice models is the appearance of a rich structure of caustics. These are regions in configuration space (=the space of the lattice field variables) where neighboring classical trajectories intersect: in the path-integral representation of the wave function the action integral does not have a minimum on the classical path but is flat along certain directions away from the classical trajectory. As a result, the integral over the Gaussian fluctuations diverges, and it is necessary to retain terms higher than the second derivative of the action integral. A systematic classification of caustics in terms of singularities of smooth mappings can be found in the literature.[5] It is also possible to construct the wave function in the vicinity of caustics.[1,6] The reason why caustics are potentially important for confinement dynamics (in the limit $g^2 \to 0$) lies in the behavior of the ground-state wave function on the caustics. In general, the semiclassical wave function $\psi(x)$ has the form

$$\psi(x) = A(x) \exp\left[-\frac{1}{g^2} S(x) + O(g^2) \right] \tag{1.2}$$

with $A(x)$ and $S(x)$ being smooth functions independent of g^2. For a point $\bar{x}$ on a caustic, however, the $g^2 \to 0$ behavior of the wave function is

$$\psi(\bar{x}) \underset{g^2 \to 0}{\sim} \text{const} \times g^{-p} \exp\left[-\frac{1}{g^2} S(\bar{x}) \right] . \tag{1.3}$$

Here p is a positive fractional number which is determined by the shape of the caustic. In a problem with a very large number of dimensions the power p can become big. If, moreover, the point $\bar{x}$ is close to the origin such that the semiclassical factor $\exp[-(1/g^2)S]$ is not too small yet, there may be some competition between the prefactor (representing quantum fluctuations) and the semiclassical factor.

In Ref. 1 we studied two extremely simple models of SU(2) lattice gauge theories: we have shown that caustics exist, and we have located and analyzed in some detail the parts of them which are closest to the origin. For the most singular pieces of the caustics (Whitney tuck and hyperbolic umbilic) we have explicitly shown how the singular behavior (1.3) arises. The models were too simple to go further: in particular, there were no exponentially small quantities whose computation could have proven the relevance of caustics.

In this paper we turn to the more realistic case of a large cubic SU(2) lattice (without fermions). Continuing along the line of argument that we have described before (for further details see also Ref. 1) we are first faced with the task of studying the flow of classical trajectories and

their caustics. In a system with such a large number of variables this first step is already rather complicated and has to be organized in several parts. We choose to work with periodic boundary conditions; it is then possible (as we will show below) to single out a lower-dimensional subspace and to study classical trajectories that stay in this subspace. It is the (nine-dimensional) space of constant (with respect to lattice sites) field configurations, i.e., of fields with zero momentum $\mathbf{k}$. This subspace already shows such a rich structure that this paper will be entirely devoted to its presentation. We see two reasons why it makes sense to start with this subspace. From a more technical point of view the analysis of classical trajectories is somewhat simpler since they stay in this subspace. In a subsequent step we will then investigate paths which are no longer confined to the $\mathbf{k}=0$ subspace but lie still close to it. Such a strategy is supported also by the physical argument that we expect long-distance phenomena to be described primarily by field configurations that are close to the $\mathbf{k}=0$ subspace. It is, therefore, desirable to have as much information as possible on these field configurations.

Interest in a semiclassical analysis of this subspace also arises from another side. A few years ago Lüscher[7] suggested studying Yang-Mills theories in a small spatial volume $V=L^3$. Because of asymptotic freedom, the region of small L can be studied through (renormalized) perturbation theory, and it was hoped that knowledge of the system at moderately small values of L would already give a reasonable approximation of the large-L behavior. However, numerical calculations[8] have shown that nonperturbative effects (e.g., tunneling between the origin and its conjugate points) are, even for small L, more important than expected and hence should be taken into account. For such an analysis one may also try to use the semiclassical approximation, and part of this would be a careful study of classical trajectories. In Refs. 9 and 10 van Baal *et al.* have studied tunneling effects between stable toron points, but this tunneling is confined to the space of toron configurations. For a complete analysis one has also to consider tunneling contributions which leave this subspace. In keeping with Lüscher's perturbation expansion one first would look in the space of constant field configuration. It is for these purposes that our results may be useful too.

Returning to our goal of locating caustics we briefly sketch our main results. In the vicinity of the origin (all field variables $\ll 1$) our Hamiltonian is invariant under rotations in both ordinary and group space and, therefore, has two sets of conserved angular momenta. Since we are interested in classical solutions with both angular momenta being zero, our originally nine-variable problem reduces to one with only three degrees of freedom. The pattern of caustics in the neighborhood of the origin is illustrated in Fig. 1. The origin sits at the top of "squeezed cones," and each of them represents a two-dimensional caustic. There are infinitely many of these "cones," one inside the other (Fig. 1 shows only two of them), and they become flatter and flatter. Their common symmetry axis is the ray $r_1=r_2>0$, $r_3=0$, and they all meet on the two rays $r_1=r_2=r_3>0$ and $r_1=r_2=-r_3>0$. A similar set of cones connects any pair of diagonal rays, e.g., $r_1=r_2=r_3>0$ with $r_1=-r_2=r_3>0$ (not shown in Fig. 1), etc. As a result, each of these diagonal rays is common to three sets of cones. Physically this "most singular" line corresponds to the following field configuration: all x-link variables point, in group space, in the one-direction, all y links in the two-direction and all z links in the three-direction.

For the ground-state wave function of the corresponding Hamiltonian operator this analysis leads to the following qualitative picture. Very close to the origin the wave function is perfectly regular—this follows from the fact that the kinetic differential operator is elliptic. Further away from the origin ("asymptotic" behavior sets in for field variables $\gg g^{2/3}$) the behavior of the wave function will be very different, depending upon whether we are outside all "cones" in Fig. 1, between the first and second, and so on. On the caustics, which are just the boundary surfaces of these regions of phase space, we have behavior like (1.3). Still further away from the origin the caustics shown on Fig. 1 will be slightly bent, but the general pattern remains. Further details will be given below.

The organization of this paper is the following. First, in Sec. II, we introduce notations and present the setup of the classical mechanics problem. In Sec. III we investigate the vicinity of the origin: there the Hamiltonian greatly simplifies due to an extra symmetry. Most of the results are obtained by analytic methods, but a few quantities have to be calculated on the computer. Section IV contains computer results on the full Hamiltonian of the $\mathbf{k}=0$ subspace. In particular, we search for solutions with finite action. In the final section we summarize and give a brief outlook.

II. DEFINITIONS AND STRATEGY

The lattice Hamiltonian for pure SU(2) Yang-Mills theory is taken from Kogut and Susskind:[2]

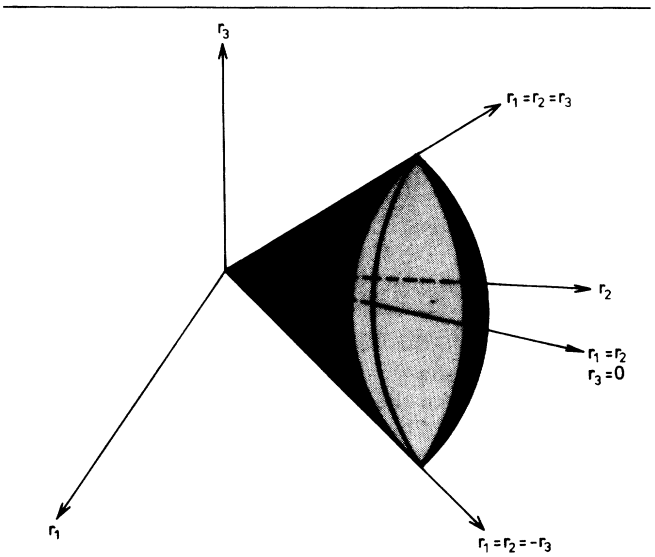

FIG. 1. Caustics in the vicinity of the origin. r_1, r_2, r_3 denote the three variables of the reduced Hamiltonian (3.9).

$$H=\frac{g^2}{2}\sum_{\text{links}}\mathbf{g}^2(\mathbf{x}_{l,i})+\frac{2}{g^2}\sum_{\text{plaquettes}}\mathrm{Tr}[1-U(\partial P)]\ . \tag{2.1}$$

We use the following notations: our cubic lattice has length $L=N$ with $N\gg 1$ but fixed, and the unit lattice spacing is set equal to 1. l denotes the site on the lattice, i the spatial direction. For each link variables we use the parametrization $U=x_0+i\boldsymbol{\sigma}\cdot\mathbf{x}$ $(x_0^2+\mathbf{x}^2=1)$. Our configuration space then consists of the points $\{\mathbf{x}_{l,i}\}$. The kinetic term has the form

$$\mathcal{J}(\mathbf{x})=\tfrac{1}{2}(x_0\mathbf{p}-\mathbf{L}),\quad \mathbf{p}=\frac{1}{i}\nabla,\quad \mathbf{L}=\mathbf{x}\times\mathbf{p}\ , \tag{2.2}$$

$$\begin{aligned}\mathcal{J}^2(\mathbf{x})mark&=\tfrac{1}{4}(-\Delta+x_a x_b\nabla_a\nabla_b+3x_a\nabla_a)\\&=-g^{ab}(\mathbf{x})(\nabla_a\nabla_b-\Gamma^c_{ab}\nabla_c)\end{aligned} \tag{2.3}$$

with the metric

$$g^{ab}(x)\equiv\tfrac{1}{4}(\delta_{ab}-x_a x_b) \tag{2.4}$$

and its Christoffel symbols $\Gamma^c_{ab}=x_c g_{ab}$. For computational purposes it is useful to have, instead of this "Cartesian" parametrization of the group manifold, "angular" variables θ, ϑ, φ:

$$\mathbf{x}=\sin\theta(\sin\vartheta\cos\varphi,\ \sin\vartheta\sin\varphi,\ \cos\vartheta)\ . \tag{2.5}$$

Then the kinetic part of (2.1) reads

$$\mathcal{J}^2=\frac{1}{4}\left[\frac{\partial^2}{\partial\theta^2}+2\cot\theta\frac{\partial}{\partial\theta}+\frac{1}{\sin^2\theta}\left[\frac{\partial^2}{\partial\vartheta^2}+\cot\vartheta\frac{\partial}{\partial\vartheta}+\frac{1}{\sin^2\vartheta}\frac{\partial^2}{\partial\varphi^2}\right]\right], \tag{2.6}$$

which is the four-dimensional Laplacian restricted to the unit sphere S_3. Throughout this paper we will use periodic boundary conditions:

$$\mathbf{x}_{l,i}=\mathbf{x}_{l+L\mathbf{e}_j,i}\ . \tag{2.7}$$

We are primarily interested in the Schrödinger equation for the ground-state wave function $\psi(\{\mathbf{x}_{l,i}\})$, which we write as

$$\left[\frac{g^4}{2}T+2V\right]\psi(\{\mathbf{x}_{l,i}\})=g^2E\psi(\{\mathbf{x}_{l,i}\})\ . \tag{2.8}$$

This form clearly exhibits the formal analogy with ordinary quantum mechanics: g^2 plays the same role as $\hbar$. When applying the semiclassical approximation to (2.8) we first divide the configuration space into classically allowed and classically forbidden regions. Under the assumption that $g^2E\to 0$ when $g^2\to 0$ (which is correct in perturbation theory) the allowed region consists of narrow "valleys" around those points for which the potential V is zero (for $g^2\to 0$, the width of these "valleys" shrinks to zero). These "toron" points[11] are those field configurations where all i links are equal (up to gauge transformations) to a constant SU(2)-matrix D_i $(i=1,2,3)$, such that $[D_i,D_j]=0$. A convenient choice is

$$D_i=\exp\left[i\sigma_3\frac{\varphi_i}{N}\right],\quad 0\le\varphi_i\le 2\pi,\quad i=1,2,3\ . \tag{2.9}$$

Configurations of the same form but with $\varphi_i\in[2\pi,4\pi]$, $\varphi_i\in[4\pi,6\pi]$, . . . are gauge equivalent to (2.9). It may be useful to illustrate this situation in Fig. 2: the toron manifold is drawn as a cube with the axes $\psi_i=\varphi_i/N$. When ψ_i ranges from 0 to π, the SU(2) element D_i moves, in group space, on S_3 from the north pole to the south pole. The value $\psi_i=\pi/2$ denotes the equator. Gauge invariance now implies that any point in this cube can be mapped into the (bigger) cube at the lower left corner. We illustrate this for two points on the three-axis: a', b' are the gauge images of a and b. It is therefore sufficient to study the "elementary cell" of toron points. In addition to gauge invariance, the Hamiltonian has a discrete group of symmetry transformations, the central conjugations.[7] Locally they are gauge transformations, but closed Wilson loops that wind around the torus pick up a phase factor (-1). Under these transformations toron points in Fig. 2 are shifted by units of π/N in the one-, two-, or three-direction (i.e., point c is mapped into c'). In particular, the eight "corner" points of the "elementary cell" (the smaller cube) are mapped onto each other: so in the vicinity of any of those eight points the Hamiltonian looks identical.

Information on the quantum system in the classically allowed region (in the limit $g^2\to 0$) has been obtained in Refs. 7 and 8. The toron valleys are widest at the eight corner points, and these points are stable in the following sense: the wave-function peaks at the corner point and then falls off sufficiently rapidly along the valley directions. As a result, the energy spectrum is discrete.[12] The

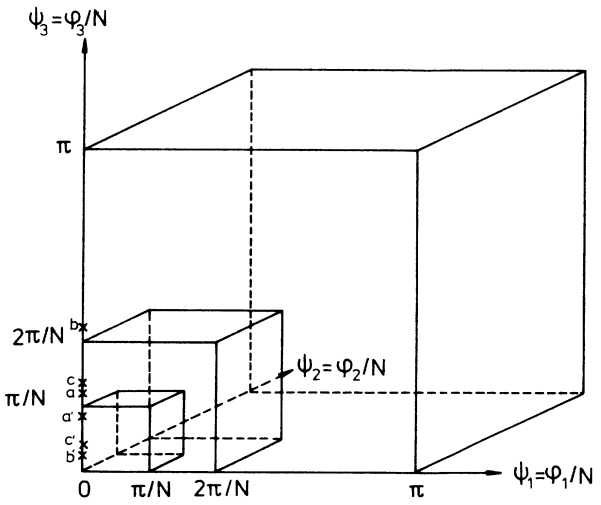

FIG. 2. The three-dimensional toron manifold: each toron point is parametrized by three angles ψ_i, $0\le\psi_i\le\pi$ $(i=1,2,3)$. Connection with Eq. (2.9) is made via $\psi_i=\varphi_i/N$. By gauge invariance, each toron point in the cube is equivalent to some point inside the small cube at the lower left corner ("elementary cube"). For example, the points a, b are gauge equivalent to a', b', respectively. The points c and c' are central conjugates of each other.

central conjugations then play a role analogous to that of reflection symmetry in a left-right-symmetric double-well potential: eigenstates of the Hamiltonian are labeled by a discrete quantum number ("electric flux"), and the degeneracy between these states will be broken only at the nonperturbative level. In the context of Lueschers approach, tunneling from one corner point to a neighboring one along the connecting (narrow) toron valley has been studied in Refs. 9 and 10. The level splitting is of the order $\exp(-1/g\times\text{const})$.

Away from the toron points we are in the classically forbidden region. For the ground-state wave function we make the ansatz

$$\psi(\{\mathbf{x}_{1,i}\})=A(\{\mathbf{x}_{1,i}\})\exp\left[-\frac{8}{g^2}S(\{\mathbf{x}_{1,i}\})\right] . \tag{2.10}$$

In order to obtain the functions A and S we have to solve the equations of motion of the classical Hamiltonian:

$$H=\tfrac{1}{2}\sum_{1,i}4g^{ab}(\mathbf{x}_{1,i})\frac{\partial S}{\partial \mathbf{x}_{1,i,a}}\cdot\frac{\partial S}{\partial \mathbf{x}_{1,i,b}}+\tfrac{1}{8}V . \tag{2.11}$$

The trajectories we are interested in have zero energy and live in Euclidean time: this is conveniently taken into account by changing in (2.11) the sign of the potential term and then using real time again. On the torons we have $S=\text{const}$; without loss of generality we choose $S=0$. All trajectories then start from toron points, and in order to calculate the wave function (2.10) at some point $\{\mathbf{x}_{1,i}\}$ away from the torons we have to know all classical trajectories which connect $\{\mathbf{x}_{1,i}\}$ with some point on the toron. As we have said before, for the moment we are mainly interested in caustics, i.e., in regions of configuration space where neighboring trajectories intersect with each other.

For a semiclassical analysis we have to solve the equations of motion which follow from (2.11):

$$\begin{aligned}&\dot{\mathbf{x}}_{1,i}=\mathbf{p}_{1,i}-\mathbf{x}_{1,i}(\mathbf{x}_{1,i}\cdot\mathbf{p}_{1,i}) ,\\ &-\dot{\mathbf{p}}_{1,i}=-\mathbf{p}_{1,i}(\mathbf{x}_{1,i}\cdot\mathbf{p}_{1,i})+\frac{1}{8}\frac{\partial V}{\partial \mathbf{x}_{1,i}} .\end{aligned} \tag{2.12}$$

For practical purposes it is important to note that the "Cartesian" parametrization of the group manifold is singular on the equator of S_3 where $|\mathbf{x}|=1$. In order to cross this line we have to switch to the "angular" variables. The corresponding equations of motion follow from (2.6).

Now it is easy to see that for constant fields, $\mathbf{x}_{1,i}=\mathbf{y}_i$, the equations of motion become much simpler:

$$\begin{aligned}&\mathbf{y}_i=\mathbf{p}_i-(\mathbf{y}_i\cdot\mathbf{p}_i)\mathbf{y}_i ,\\ &\dot{\mathbf{p}}_i=(\mathbf{y}_i\cdot\mathbf{p}_i)\mathbf{p}_i+[\mathbf{y}_i(\mathbf{y}_1^2+\mathbf{y}_2^2+\mathbf{y}_3^2)-\mathbf{y}_1(\mathbf{y}_i\cdot\mathbf{y}_1)\\ &\qquad -\mathbf{y}_2(\mathbf{y}_2\cdot\mathbf{y}_i)-\mathbf{y}_3(\mathbf{y}_3\cdot\mathbf{y}_i)] .\end{aligned} \tag{2.13}$$

The rotation symmetry (in group space) is the leftover of gauge invariance. It is this set of equations of motion that we shall discuss in the rest of this paper. The Hamiltonian which belongs to it is

$$\begin{aligned}H=&\tfrac{1}{2}\sum_i[\mathbf{p}_i^2-(\mathbf{y}_i\cdot\mathbf{p}_i)^2]\\ &+\tfrac{1}{2}[\mathbf{y}_1^2\mathbf{y}_2^2-(\mathbf{y}_1\cdot\mathbf{y}_2)^2+\mathbf{y}_1^2\mathbf{y}_3^2-(\mathbf{y}_1\cdot\mathbf{y}_3)^2\\ &+\mathbf{y}_2^2\mathbf{y}_3^2-(\mathbf{y}_2\cdot\mathbf{y}_3)^2] .\end{aligned} \tag{2.14}$$

III. VICINITY OF THE ORIGIN

It is natural to start the investigation in the region of small fields $|\mathbf{y}_i|\le\pi/N\ll 1$, i.e., in the vicinity of the toron point (2.9) with $\varphi_1=\varphi_2=\varphi_3=0$, the origin. In this region we can neglect the nontrivial piece of the metric tensor (2.4), and our problem simplifies,

$$\begin{aligned}H=&\tfrac{1}{2}(\mathbf{p}_1^2+\mathbf{p}_2^2+\mathbf{p}_3^2)+\tfrac{1}{2}[\mathbf{y}_1^2\mathbf{y}_2^2-(\mathbf{y}_1\cdot\mathbf{y}_2)^2+\mathbf{y}_1^2\mathbf{y}_3^2-(\mathbf{y}_1\cdot\mathbf{y}_3)^2\\ &+\mathbf{y}_2^2\mathbf{y}_3^2-(\mathbf{y}_2\cdot\mathbf{y}_3)^2] ,\end{aligned} \tag{3.1}$$

leading to the equations of motion:

$$\ddot{\mathbf{y}}_i=\mathbf{y}_i(\mathbf{y}_1^2+\mathbf{y}_2^2+\mathbf{y}_3^2)-\mathbf{y}_1(\mathbf{y}_1\cdot\mathbf{y}_i)-\mathbf{y}_2(\mathbf{y}_2\cdot\mathbf{y}_i)-\mathbf{y}_3(\mathbf{y}_3\cdot\mathbf{y}_i) . \tag{3.2}$$

[For the equations of motion (3.2) we have already taken into account that we are looking for solutions with imaginary time: when deriving (3.2) from (3.1), we first change the sign of the potential.] The Hamiltonian (3.1) has been studied before[13–19] and we can be brief in stating the main results.

The Hamiltonian has two kinds of rotation symmetries: rotations in group space which correspond to gauge transformations in the $\mathbf{k}=0$ subspace and, in addition, rotations in ordinary space. This second symmetry can most easily be seen if we write the potential as $\frac{1}{2}\epsilon^{abc}\epsilon^{ab'c'}y_{ib}y_{jc}y_{ib'}y_{jc'}$. Let Y denote the 3×3 matrix

$$Y=(\mathbf{y}_1,\mathbf{y}_2,\mathbf{y}_3)=\begin{pmatrix}y_{11}&y_{21}&y_{31}\\ y_{12}&y_{22}&y_{32}\\ y_{13}&y_{23}&y_{33}\end{pmatrix} . \tag{3.3}$$

Rotation in group space then corresponds to multiplication by an orthogonal matrix from the left, whereas rotation in ordinary space is obtained by matrix multiplication from the right. A general field configuration Y is conveniently parametrized by

$$Y=O_L R O_R^T , \tag{3.4}$$

where the diagonal matrix R has three independent entities, and O_L and O_R depend upon three Euler angles each. Each rotation symmetry has its own conserved angular momenta:

$$M_i=\epsilon_{ijk}y_{ja}y_{ka} , \tag{3.5}$$

$$N_a=\epsilon_{abc}y_{ib}y_{ic} . \tag{3.6}$$

They have vanishing Poisson brackets:

$$[M_i,N_a]_{\mathrm{PB}}=0 . \tag{3.7}$$

Since we want gauge-invariant quantities, we always requires $\mathbf{N}=0$. Classical solutions to (3.2) with energy zero

which leave from a toron point require also $\mathbf{M}=0$. We therefore can restrict ourselves to matrices Y [Eq. (3.3)] and P:

$$P=(\mathbf{p}_1,\mathbf{p}_2,\mathbf{p}_3)\ , \tag{3.8}$$

which are diagonal. Our nine-dimensional Hamiltonian system thus reduces to a three-dimensional "reduced" Hamiltonian:

$$H=\tfrac{1}{2}(p_1^2+p_2^2+p_3^2)+\tfrac{1}{2}(r_1^2r_2^2+r_1^2r_3^2+r_2^2r_3^2)\ . \tag{3.9}$$

Despite its simple-looking form, this Hamiltonian is nonintegrable.[8,15,16,19] There are no integrals of motion other than the energy, and the system is stochastic[17] (Kolmogorov K system). All these results initially only apply to the classical allowed region, but they can be translated into the classically forbidden region.

Before we discuss in detail classical trajectories of the Hamiltonian (3.9), a few words should be said about the quantum mechanics of (3.1) (with the factor $g^2/4$, $4/g^2$ reinserted in front of the kinetic part and the potential, respectively). The symmetries can be used[20] to reduce, for the ground-state wave function, the Hamiltonian to (3.9) (with appropriate factors of g^2). It is known[7,12] that this Hamiltonian has a discrete energy spectrum, but so far no analytic solution for the wave function is known. For small r_i it is a regular function (because of the elliptic nature of the differential operator). The semiclassical analysis in the classically forbidden region will be valid as long as we stay sufficiently far away from the boundary between the allowed and forbidden zone:

$$|r_i| \gg g^{2/3}\ . \tag{3.10}$$

(We could also have eliminated the g^2 dependence altogether by rescaling $r_i \to r_i'=r_i g^{-2/3}$; then our analysis applies to the "asymptotic" region $|r_i'| \gg 1$).

Let us now turn to a study of classical trajectories of the Hamiltonian (3.9). Once again, since we are interested in the classically forbidden region, we simply change the sign of the potential. The equations of motion to be solved are

$$\ddot{r}_1=r_1(r_2^2+r_3^2),\quad \ddot{r}_2=r_2(r_1^2+r_3^2),\quad \ddot{r}_3=r_3(r_1^2+r_2^2)\ . \tag{3.11}$$

Toron points lie on the r_1 or r_2 or r_3 axis. We first ask for solutions which stay in the r_1-r_2 plane [$r_3\equiv 0$ is a solution to (3.11)]. It is easy to see that the only way to leave the origin is along the 45° lines $r_1=r_2$ or $r_1=-r_2$: $r_1=r_2=\sqrt{2}/(-t)$ is an exact solution. By linearizing the equations of motion around this solution one finds that neighboring solutions come closer if one moves away from the origin but diverge if one moves towards the origin. To lowest order we have

$$r_{1,2} \underset{t\to 0^-}{\sim} \frac{\sqrt{2}}{-t}\{1\pm A\sqrt{-t}^{\,3}\sin[\tfrac{1}{2}\sqrt{7}\ln(-t)]\}\ . \tag{3.12}$$

These solutions oscillate around the ray $r_1=r_2>0$, and the amplitude of oscillations decreases for $t\to 0^-$ (i.e., $r_1=r_2\to\infty$). Following one of the paths backwards in time (i.e., towards the origin), the oscillations become stronger until finally the perturbative treatment becomes invalid. On the other hand we know that paths depart from the r_1 axis (or r_2 axis) at 90°: there are no forces parallel to the axis. These two pieces of information are sufficient to understand the qualitative form of classical trajectories; more detailed properties are obtained from a computer analysis. Results are shown in Fig. 3. Figure 3(a) gives a schematic illustration of a few classical trajec-

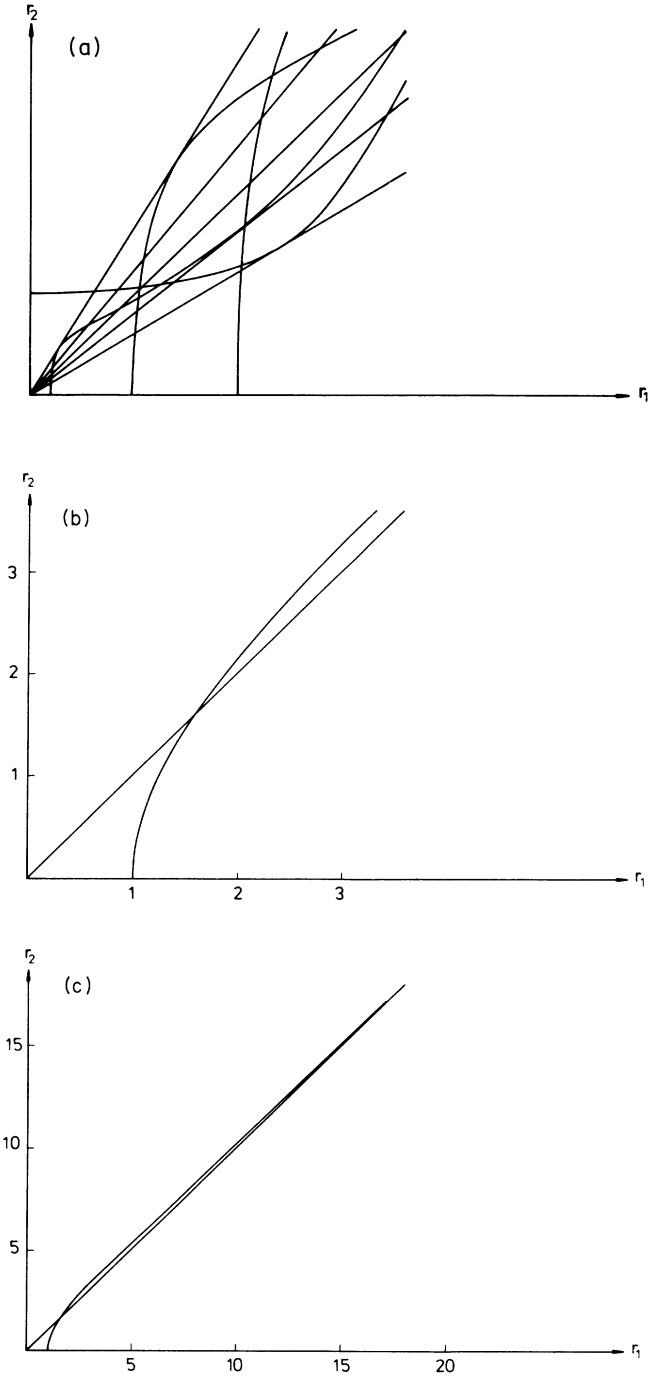

FIG. 3. (a) Schematic pattern of classical trajectories in the r_1-r_2 plane. (b) A classical trajectory of (3.9) in the r_1-r_2 plane. (c) The same as (b), but a different scale in r_1 and r_2.

tories: each of them departs from the r_1 axis at 90°, moves upwards towards the 45° line $r_1=r_2$, crosses it, reaches a maximal distance from it, returns, and then follows the oscillations described by (3.12). In Figs. 3(b) and 3(c) we present the computer analysis of a single path which leaves from the toron point $(r_1,r_2)=(1,0)$. In Fig. 3(c) already the second oscillation is too small to be visible. The next ingredient to note is that a common scaling of r_1 and r_2 can be compensated by a rescaling of time t: therefore all trajectories which leave the r_1 axis have the same form [Fig. 3(a)], and it suffices to compute only one single path. Maxima of oscillations of all trajectories lie on rays which intersect at the origin. Because of symmetry under $r_1 \leftrightarrow r_2$ these rays come in pairs. Below we shall see that each pair of rays represents the section of a cone with the r_1-r_2 plane. From (3.12) it follows that there are infinitely many of such pairs, with opening angles tending to zero very rapidly. In Table I (last column) we give the angles of the eight largest ones.

Because of the scaling property mentioned before there is really only one trajectory to be calculated; i.e., all information is contained in one function. A convenient way of defining this function is the following. From the two equations of motion it is possible to eliminate, by using conservation of energy, the variable time and to consider one of the r's as function of the other one. More conveniently, put $r_1=e^{\xi}\cos\varphi$, $r_2=e^{\xi}\sin\varphi$ and consider $f_1=\sin\varphi$ as function of ξ. The differential equation for f_1 becomes

$$f_1''=\frac{-f_1}{1-f_1^2}f_1'^2-3f_1'\left[1+\frac{f_1'^2}{1-f_1^2}\right]+\frac{1-2f_1^2}{f_1}\left[1+\frac{f_1'^2}{1-f_1^2}\right], \tag{3.13}$$

where $f_1'=df_1/d\xi$. As an initial point we choose $r_1=1$, $r_2=0$, i.e., $\xi=0$, $f_1=0$. For large ξ, f_1 then approaches the limiting value $\frac{1}{2}\sqrt{2}$ (Fig. 4). The analogue of (3.12) is

$$f_1 \underset{\xi\to\infty}{\sim} \frac{1}{2\sqrt{2}}+A'e^{-(3/2)\xi}\sin(\tfrac{1}{2}\sqrt{7}\xi-\varphi_0)\,. \tag{3.14}$$

Table I contains the values of f_1 at the first eight extremal points; in Fig. 4 we also indicate that the asymptotic form (3.14) fits the function f_1 extremely well: deviations become visible only at the first maximum.

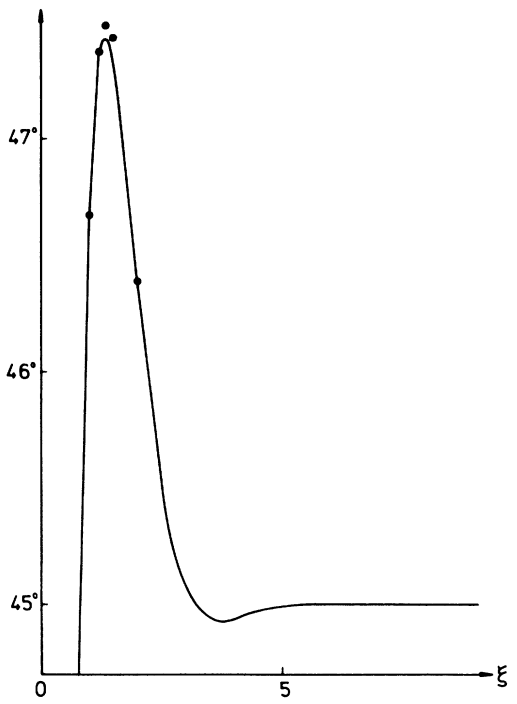

FIG. 4. A classical trajectory of (3.9) in the r_1-r_2 plane [same as Fig. 3(b) and 3(c)]: we use the parametrization $r_1=e^{\xi}\cos\varphi$, $r_2=e^{\xi}\sin\varphi$, and we plot φ as a function of ξ. Oscillations to the right of $\xi=5$ are too small to be visible. For $\xi>2$ the curve is well approximated by (3.13) with $A'=0.340\,271\,935\,26$, $\varphi_0=12.617\,681\,540\,62$. The small dots drawn in Fig. 4 illustrate how this approximation starts to deviate for $\xi<2$.

From our discussion it follows that the rays in Fig. 3(a) are lines of caustics. They are envelopes to the maxima of oscillations of neighboring trajectories. A point which lies outside of all pairs of rays can be connected by exactly one trajectory with a toron point, either on the r_1 or r_2 axis. For points between the first and the second pair there are already three such paths, between the second and third pair there are five paths, and so on. Each of the caustic lines has the characteristic of the fold.[5] It is possible to construct the wave function in the vicinity of each caustic, but this will not be discussed here in further detail. The main features that we want to stress here are the following. (i) There is a denumerable set of infinitely

TABLE I. Opening angles for the eight largest cones of caustics. We use $r_1=e^{\xi}\cos\varphi$, $r_2=e^{\xi}\sin\varphi$ and follow the oscillations of a single trajectory around the ray $\varphi=45°$. The first column contains the values of ξ for which the first, second, ... oscillation reaches its maximum. In the other columns we give the corresponding φ value. The opening angles of the cones $2\,|\,45°-\varphi\,|$ are contained in the last column.

ξ	$\sin\varphi$	φ	2φ	$2\,\lvert 45°-\varphi\rvert$
1.3435	0.736 485 201 263	47.432 863 097 567	94.865 736 195 134	4.9°
3.7165	0.706 253 330 875	44.930 887 894 296	89.861 775 788 591	1.4×10^{-1}°
6.0915	0.707 130 983 228	45.001 961 087 887	90.003 922 175 773	3.9×10^{-3}°
8.4660	0.707 106 094 431	44.999 944 353 247	89.999 888 706 494	1.1×10^{-4}°
10.8410	0.707 106 800 674	45.000 001 579 000	90.000 003 158 000	3.1×10^{-6}°
13.2160	0.707 106 780 634	44.999 999 955 194	89.999 999 910 389	9.0×10^{-8}°
15.5910	0.707 106 781 202	45.000 000 001 271	90.000 000 002 541	2.5×10^{-9}°
17.9585	0.707 106 781 186	44.999 999 999 963	89.999 999 999 926	7.4×10^{-11}°

many caustic lines which accumulate on the ray $r_1=r_2$. (ii) Caustics do not start at some finite distance away from the origin (as it was the case in the simple models of Ref. 1) but begin right at the origin [note, however, the condition (3.10) and the discussion before]. All this makes it likely that these caustics will play an important role in the dynamics of lattice gauge theories.

Next we leave the r_1-r_2 plane. In particular, we want to know how the caustic lines in the r_1-r_2 plane become part of surfaces intersecting the r_1-r_2 plane. Again we begin by asking which trajectories come out of the origin. The only directions are the line $r_1=r_2=r_3$ (by symmetry, also the lines $r_1=r_2=-r_3$, etc.), the line $r_1=r_2$ in the r_1-r_2 plane which we have studied before, and paths in the plane $r_1=r_2$ which leave the origin infinitesimally close to the direction $r_3=0$ but then deviate from it. As to the first possibility, $r_1=r_2=r_3=1/(-t)$ is an exact solution. Linearization of the equations of motion around this path shows that all solutions in the vicinity approach the ray $r_1=r_2=r_3$ in the direction away from the origin but deviate from it when moving towards the origin. In contrast with (3.12), there are no oscillations:

$$r_i(t) \underset{t\to 0^-}{\sim} \frac{1}{-t}(1+\alpha_i t^2+ct^4), \quad \alpha_1+\alpha_2+\alpha_3=0 . \tag{3.15}$$

In the half-plane $r_1=r_2>0$ we have, close to the ray $r_1=r_2$, $r_3=0$ the perturbative solution

$$r_1=r_2=\frac{\sqrt{2}}{-t}, \quad r_3=\frac{\text{const}}{(-t)^{(\sqrt{17}-1)/2}} . \tag{3.16}$$

For $t\to-\infty$ (i.e., towards the origin) it approaches the ray $r_1=r_2$, $r_3=0$; for $t\to 0$ it moves upwards and eventually approaches the line $r_1=r_2=r_3$ according to (3.15). A computer result for such a path is shown in Fig. 5 (lower curve). This exhausts the trajectories which come out of the origin, and further details are gained only with the help of the computer.

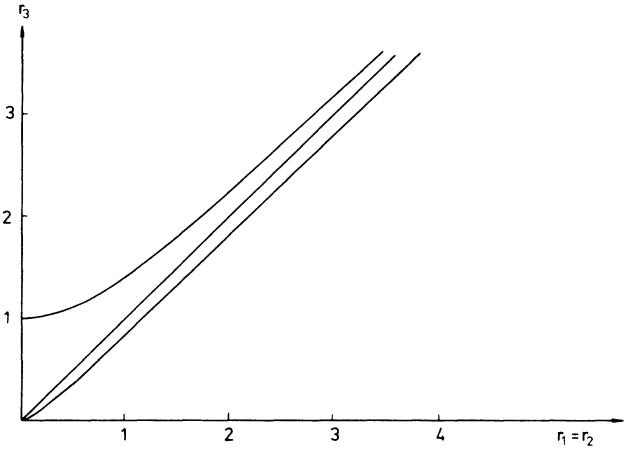

FIG. 5. Classical trajectories of (3.9) in the plane $r_1=r_2>0$, $r_3>0$. The straight line is the solution $r_1=r_2=r_3=1/(-t)$.

Instead of integrating the equations of motion (3.11) it is again more convenient to first eliminate time t, using energy conservation, then to express two variables as functions of the third one. We choose $r_1=e^{\xi}\sin\vartheta\cos\varphi$, $r_2=e^{\xi}\sin\vartheta\sin\varphi$, $r_3=e^{\xi}\cos\vartheta$ and express $f_1=\sin\varphi$, $f_2=\cos\vartheta$ as function of ξ. The resulting equations are

$$\begin{aligned} f_1'' = {} & \frac{-f_1}{1-f_1^2}f_1'^2-3f_1'\left[1+\frac{f_2'^2}{1-f_2^2}+(1-f_2^2)\frac{f_1'^2}{1-f_1^2}\right]+2\frac{f_2}{1-f_2^2}f_1'f_2' \\ & +\left[1+\frac{f_2'^2}{1-f_2^2}+(1-f_2^2)\frac{f_1'^2}{1-f_1^2}\right]\frac{f_1(1-f_1^2)(1-2f_2^2)}{f_1^2(1-f_1^2)(1-f_2^2)+f_2^2} , \end{aligned} \tag{3.17}$$

$$\begin{aligned} f_2'' = {} & \frac{-f_2}{1-f_2^2}f_2'^2-3f_2'\left[1+\frac{f_2'^2}{1-f_2^2}+(1-f_2^2)\frac{f_1'^2}{1-f_1^2}\right]-f_2(1-f_2^2)\frac{f_1'^2}{1-f_1^2} \\ & -\left[1+\frac{f_2'^2}{1-f_2^2}+(1-f_2^2)\frac{f_1'^2}{1-f_1^2}\right]f_2\frac{2(1-f_2^2)f_1^2(1-f_1^2)+2f_2^2-1}{f_1^2(1-f_1^2)(1-f_2^2)+f_2^2} . \end{aligned} \tag{3.18}$$

After linearization near the line $r_1=r_2=r_3$, i.e., $f_1=\sin\varphi=1/\sqrt{2}$, $f_2=\cos\vartheta=1/\sqrt{3}$, we find

$$\begin{aligned} f_1 &= \frac{1}{\sqrt{2}}+\alpha_1 e^{-\xi}+\beta_1 e^{-2\xi} , \\ f_2 &= \frac{1}{\sqrt{3}}+\alpha_2 e^{-\xi}+\beta_2 e^{-2\xi} , \end{aligned} \tag{3.19}$$

with some constants α_1, α_2, β_1, β_2. From (3.19) one sees, in particular, that for $\xi\to\infty$ the classical path approaches the ray $r_1=r_2=r_3>0$ inside a certain plane where orientation is given by the choice of α_1, α_2.

As a result of a computer analysis of Eq. (3.17) and (3.18) we first discuss what the caustics look like. In Fig. 6 we show, for two examples, how the angles φ of the rays of Fig. 3(a) vary when we leave the plane $r_3=0$ ($\vartheta=90°$): they start with the values given in Table I. When we turn on r_3 ($\vartheta<90°$), the angles φ start to move towards 45°. This limiting value is reached when $\cos^2\vartheta=1/\sqrt{3}$ or $\vartheta=54.73\ldots°$. The limiting slope of $\vartheta(\varphi)$ is finite. It then follows (Fig. 1) that the caustics have the form of "squeezed" cones, with the top at the origin. They all meet at the two rays $r_1=r_2=r_3>0$ and

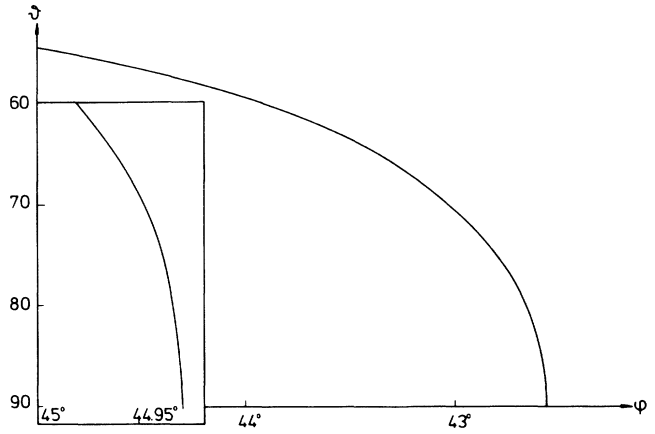

FIG. 6. Cross sections of the two largest cones of caustics (cf. Fig. 1). Using the parametrization $r_1=e^{\xi}\sin\vartheta\cos\varphi$, $r_2=e^{\xi}\sin\vartheta\sin\varphi$ we plot ϑ vs φ. For the smaller cone we have used a different scale (inside the box).

$r_1=r_2=-r_3>0$, and their common symmetry axis is the ray $r_1=r_2>0$, $r_3=0$. There are infinitely many of them, one inside the other, and asymptotically they become flat, converging towards the plane $r_1=r_2>0$, $-r_1\le r_3\le r_1$. By symmetry, similar sets of cones connect the ray $r_1=r_2=r_3>0$ also with the rays $r_1=-r_2=r_3>0$ and $-r_1=r_2=r_3>0$, and similarly for all the other diagonal rays. As a result, each of these rays is common to three sets of caustic cones, and in this sense these directions away from the origin are the most singular ones.

We finally discuss, qualitatively, the behavior of trajectories which leave a toron point, say on the positive r_1 axis. If the trajectory leaves exactly inside the plane $r_3=0$, it will stay there forever, and its shape has been discussed before [Figs. 3(a) and 3(b)]. Whenever it starts to return towards the asymptotic direction $r_1=r_2$, it hits one of the caustic cones. If our trajectory starts with a very small angle in the positive r_3 direction, it will follow, for a long time, the motion inside the plane $r_3=0$. Eventually it will be very close to the plane $r_1=r_2$ and then follow the motion inside this plane (Fig. 5): it rises upwards and eventually approaches the ray $r_1=r_2=r_3>0$. The larger the initial angle was, the faster will the trajectory rise in r_3 direction, and, in the asymptotic form (3.19), α_1 grows compared to α_2. A look at Fig. 6 shows that our trajectory will, asymptotically, run between two caustics: it has not performed enough oscillations in order to reach the inner caustics. By further increasing the initial angle, we eventually reach the situation that our trajectory runs in the plane $r_2=r_3$: here it has the same form as the upper curve in Fig. 5. There are no oscillations at all. Figure 6 has been obtained by following, while increasing the initial angle, the oscillations around the direction $r_1=r_2$ which we had found first in the plane $r_3=0$.

IV. FURTHER AWAY FROM THE ORIGIN

So far our analysis has been restricted to the vicinity of the origin: $|\mathbf{y}_i|\le\pi/N\ll 1$. Because of the scaling properties of the reduced Hamiltonian (3.9) the structure of caustics starts right at the origin on an infinitesimally small scale. In this section we want to consider trajectories further away from the origin.

First we comment on classical trajectories which leave from toron points outside the "elementary cell" in Fig. 2 [but still inside that region where the reduced Hamiltonian (3.9) is a valid approximation]. As we have said before, such toron points can always be mapped onto the interior of the elementary cell, either by gauge transformations or by conjugacy transformations. To be more specific, consider points on the three-axis in Fig. 2. A conjugation which maps the interval $[\pi/N,2(\pi/N)]$ onto $[0,\pi/N]$ has the form

$$C_1=\exp\left[i\sigma_3 l_3\frac{\pi}{N}\right]. \tag{4.1}$$

Similarly, a gauge transformation, which transforms the interval $[2\pi/N,3(\pi/N)]$ onto $[0,\pi/N]$, is given by

$$U_l=\exp\left[i\sigma_3 l_3\frac{2\pi}{N}\right]. \tag{4.2}$$

Both (4.1) and (4.2) are l_3 dependent and, hence, map constant field configurations (with $\mathbf{k}=0$) onto those with some $\mathbf{k}\neq 0$. In the case of (4.1), fields with $\mathbf{k}=0$ acquire components with $\mathbf{k}=(0,0,\pm 2\pi/N)$. In particular, a trajectory which leaves a toron point $\sin\pi/N<r_3<\sin 2\pi/N$ in the $\mathbf{k}=0$ subspace (and then stays there forever) is mapped onto a trajectory which leaves from a toron point inside the elementary cell in the direction of fields with $\mathbf{k}=(0,0,\pm 2\pi/N)$. The same holds for (4.2), but now $\mathbf{k}=(0,0,\pm 4\pi/N)$. So our analysis of trajectories in the $\mathbf{k}=0$ subspace, when extended to starting points outside the elementary cell, gives information on trajectories close to the origin which leave in the direction $\mathbf{k}\neq 0$. A detailed analysis of these trajectories will not be given here. We only note one important feature. Fig. 3(a) shows that a trajectory in the r_1-r_2 plane which leaves from the r_1 axis somewhat away from the origin, say from $r_1=\sin\psi_1$ with $2\pi/N<\psi_1<3\pi/N$, will always intersect with any trajectory on the r_1-r_2 plane which starts closer to the origin. [Note the slight change in notation: according to Eq. (2.9) and the discussion in Sec. II, on a toron point field variables point in the three-direction. In the previous Sec. III, however, we have, for simplicity, considered toron points on the r_1 axis which corresponds to the one-direction in group space.] In particular, this applies to that trajectory which leaves from $r_1'=\sin\psi_1'$ with $\psi_1'=\psi_1-2\pi/N$: this is the image point of r_1 under the gauge transformation analogous to (4.2). This implies that the two trajectories which leave from r_1, one in the direction of $\mathbf{k}=0$, the other one $\mathbf{k}=(0,0,\pm 4\pi/N)$, initially move in different directions and separate from each other. After a while, they intersect again, if we identify points which are connected via gauge transformations. This clearly indicates that there are more caustics intersecting with the $\mathbf{k}=0$ subspace than we have located in the previous section, and some of them start at finite distances away from the origin.

Next we leave the region of small fields $|\mathbf{y}_i| \ll 1$ and return to the full Hamiltonian (2.14). Because of the second part of the metric tensor we no longer have the symmetry of rotations in ordinary space, and also the scaling symmetry is lost. So the caustics will be slightly deformed when the $|y_i|$ come close to unity, and these deformations will depend upon the direction in which we go away from the origin. Rather than discussing this in much detail we will concentrate on another aspect which is of strongest interest in connection with our semiclassical analysis of a quantum system: the search for classical solutions with finite action. From Refs. 5 and 21 we know, for the reduced Hamiltonian (3.9) in the classically allowed region, that classical motion is ergodic. In particular, trajectories are very sensitive to a change in the initial conditions. Two trajectories which initially are very close may, after some time, depart very far from each other. One expects that these properties also apply to the full Hamiltonian (2.14) in the forbidden region. Therefore, a trajectory which at time $t=-\infty$ departs from some toron point almost certainly will not end at some other toron point, but it will wander around without ever coming to rest. Only a very small subset of these trajectories has a chance to end on some toron point and, hence, to have a finite action integral. In the following we shall search for a few such solutions. For simplicity, we restrict ourselves to the vicinity of those two "obvious" solutions which already in the previous section have played an important role. These are the distinctive solutions which come out of the origin and then run along one of the rays $r_1=r_2=r_3>0$ or $r_1=r_2>0$, $r_3=0$. It is easily seen that they remain exact solutions also of the full Hamiltonian (2.14). We shall see that there are solutions with finite action close to the ray $r_1=r_2>0$, $r_3=0$, and our discussion will be limited to them. In particular, we demand also that the action integral will be close to that taken along this ray.

Let us start with the classical trajectories which come out of the origin. The most symmetric one runs along the ray $r_1=r_2=r_3>0$ (in the language of the reduced Hamiltonian) or, in the $\mathbf{y}_i$ variables (3.3):

$$Y=\begin{bmatrix} r & 0 & 0 \\ 0 & r & 0 \\ 0 & 0 & r \end{bmatrix} . \tag{4.3}$$

For the function $r(t)$ and its action integral we find

$$r(t)=\frac{1}{(1+t^2)^{1/2}} , \tag{4.4}$$

$$S=N^3\int_{-\infty}^{\infty}\sum_i(\mathbf{p}_i\cdot\dot{\mathbf{y}}_i)dt=3N^2\frac{\pi}{2} . \tag{4.5}$$

For $t\to\infty$ the path ends at the corner point opposite to the origin (Fig. 2), namely, $\psi_1=\psi_2=\psi_3=\pi$. It is gauge equivalent either to the origin itself or the corner point $(\pi/N,\pi/N,\pi N)$ of the elementary cube. A computer analysis shows that in the vicinity of this path there are no solutions with finite action close to (4.5). From the discussion in Sec. III we know that the path (4.3) is attractive: all solutions which start at some toron point in the vicinity of the origin (with the exception of those which stay in the planes $r_1=0$ or $r_2=0$ or $r_3=0$) approach this line. But before they can reach it, the nontrivial part of the metric [which makes the difference between (3.9) and (2.14)] becomes important and forces the solution (4.3) back towards $r\to 0$. Trajectories which initially are very close to (4.3) follow this general behavior, but, shortly before (4.3) reaches its end point, they diverge away from it and miss the toron subspace.

The other "obvious" solution runs along the diagonal ray in the plane, say the r_1-r_2 plane:

$$Y=\begin{bmatrix} r & 0 & 0 \\ 0 & r & 0 \\ 0 & 0 & 0 \end{bmatrix} \tag{4.6}$$

with

$$r(t)=\frac{1}{[1+(t/\sqrt{2})^2]^{1/2}} \tag{4.7}$$

and

$$S=N^3\int_{-\infty}^{\infty}\sum_i(\mathbf{p}_i\cdot\dot{\mathbf{y}}_i)dt=N^3\sqrt{2}\frac{\pi}{2} . \tag{4.8}$$

This trajectory ends at the corner point $(\pi,\pi,0)$ in Fig. 2. Now consider a solution which leaves a toron point on the r_1 axis close to the origin:

$$Y=\begin{bmatrix} r_1(t) & 0 & 0 \\ 0 & r_2(t) & 0 \\ 0 & 0 & 0 \end{bmatrix} \tag{4.9}$$

with $r_2(t)\to 0$ for $t\to-\infty$. From the previous section we know that this solution approaches the solution (4.6) and then oscillates around it. With increasing time t the oscillations are getting smaller and smaller. In the Hamiltonian (2.14) they have time for only a finite number of oscillations, before $r(t)$ in (4.6) reaches the equator $r=1$ and then starts to decrease again. Solution (4.9) continues to oscillate with again increasing oscillations, but when (4.6) reaches its end point, these oscillations are, in general, out of phase such that no toron point is reached. If, however, just on the equator the oscillations happen to pass through (4.6), i.e., the two vectors $\mathbf{y}_1(t)$ and $\mathbf{y}_2(t)$ simultaneously cross their respective equator, and the solution (4.9) looks the same on both sides of the equator, then the solution will also end at a toron point, and we have a solution with finite action. In Fig. 7 we schematically illustrate a few examples: if the starting point moves closer to the origin, the solution performs more oscillations, and there exists a infinite set of such finite action paths. Moving the starting point in the opposite direction we eventually arrive at the extreme case [(c) of Fig. 7]:

$$Y=\begin{bmatrix} 1 & 0 & 0 \\ 0 & r_2(t) & 0 \\ 0 & 0 & 0 \end{bmatrix}, \quad r_2(t)=2\frac{e^t}{1+e^{2t}} \tag{4.10}$$

with the action integral

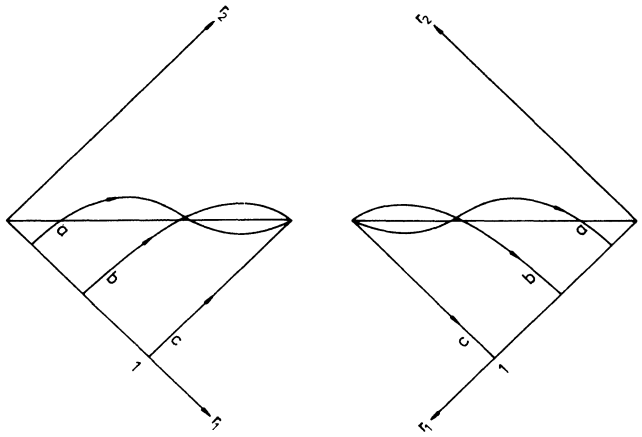

FIG. 7. Examples of trajectories with finite action for the Hamiltonian (2.14): $\mathbf{y}_1(t)=(r_1(t),0,0)$, $\mathbf{y}_2(t)=(0,r_2(t),0)$, $\mathbf{y}_3(t)=(0,0,0)$. The left half shows the "northern hemisphere" of $\mathbf{y}_1$, $\mathbf{y}_2$, the right half the "southern hemisphere." The horizontal line represents the solution $r_1=r_2=\sqrt{2}/(-t)$, line (c) belongs to (4.10). Trajectories (b) and (c) have the property that on the "equator" ($|\mathbf{y}_1|=1$, $|\mathbf{y}_2|=1$) they intersect with the line $r_1\equiv r_2$: that is why they are symmetric on both sides of the equator and start and end on toron points. All trajectories are schematic.

$$S=N^3 2\ . \tag{4.11}$$

Comparison with (4.8) shows that the oscillating paths are "shorter" than the straight line (4.6). Further investigation shows that there exists still another set of solutions of the form (4.9) which also end at toron point and, hence, have finite action. Here $\mathbf{y}_1$ and $\mathbf{y}_2$ do not pass at the same time across the equator, but still there is a symmetry between the two sides of the equators.

Next, consider another set of trajectories in the vicinity of (4.3). From (4.9) it differs by a spatial rotation (= matrix multiplication from the right, 45° rotation in the x-y plane):

$$Y=\begin{pmatrix} r_1 & r_1 & 0 \\ -r_2 & r_2 & 0 \\ 0 & 0 & 0 \end{pmatrix} \tag{4.12}$$

[again $r_2(t)\to 0$ for $t\to-\infty$]. These solutions start from toron points with $\mathbf{y}_1=\mathbf{y}_2$. For small r_1 and r_2 the motion is described by the reduced Hamiltonian (3.9) which is invariant under spatial rotations. The functions r_1 and r_2, therefore, evolve as in the previous case. However, when r_1 and r_2 grow the Hamiltonian looses the symmetry under spatial rotations, and (4.10) and (4.12) evolve differently. Nevertheless, our previous discussion still applies: (4.2) oscillates around the solution

$$Y=\begin{pmatrix} r & r & 0 \\ -r & r & 0 \\ 0 & 0 & 0 \end{pmatrix} \tag{4.13}$$

which is gauge equivalent to (4.6). In general, a trajectory (4.12) will not end at a toron point. Candidates for solutions with finite action are those trajectories which on the equators of $\mathbf{y}_1$ and $\mathbf{y}_2$ have certain symmetry properties. Since (4.12) already implies $|y_1|=|y_2|=\sqrt{r_1^2+r_2^2}$, the oscillating quantity is $(\mathbf{y}_1\cdot\mathbf{y}_2)/|y_1|\,|y_2|=\cos\varphi$ (it oscillates around 90°). We therefore demand that, on the equator, either φ passes through 90° or $\dot\varphi=0$. For the first case a few examples are shown in Fig. 8. For starting points close to the origin these trajectories have more and more oscillations, and their action integral approaches (4.8). At the opposite end, the trajectory with the smallest number of oscillations [(c) of Fig. 8] can be found analytically:

$$r_1(t)=\frac{1}{(1+e^{2\sqrt{2}t})^{1/2}}\ ,\qquad r_2(t)=\frac{e^{\sqrt{2}t}}{(1+e^{2\sqrt{2}t})^{1/2}}\ . \tag{4.14}$$

Its action integral

$$S=N^3\sqrt{2} \tag{4.15}$$

is, again, smaller than (4.8), i.e., the oscillating paths are "shorter" than the straight line (4.6) with (4.7).

A very similar discussion applies to a larger class of trajectories which interpolates between (4.9) with (4.12):

$$Y=\begin{pmatrix} \cos\alpha & -\sin\alpha & \\ \sin\alpha & \cos\alpha & \\ & & 1 \end{pmatrix}\begin{pmatrix} r_1 & & \\ & r_2 & \\ & & 0 \end{pmatrix}\begin{pmatrix} \cos\beta & \sin\beta & \\ -\sin\beta & \cos\beta & \\ & & 1 \end{pmatrix} \tag{4.16}$$

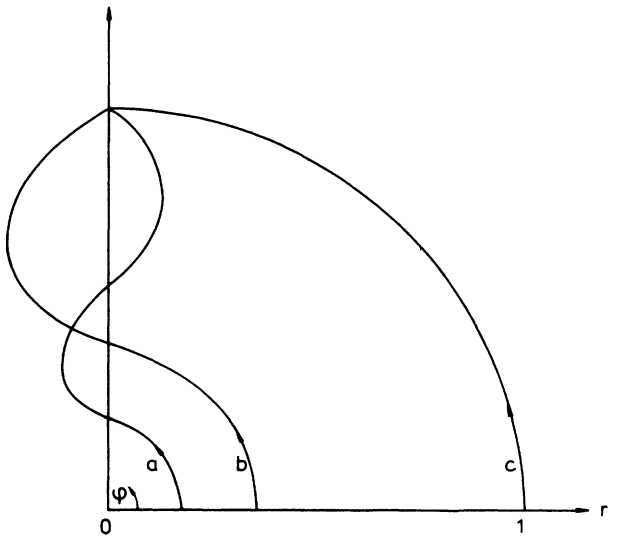

FIG. 8. Other examples of trajectories with finite action for the Hamiltonian (2.14): $\mathbf{y}_1(t)=(r_1(t),-r_2(t),0)$, $\mathbf{y}_2(t)=(r_1(t),r_2(t),0)$, $\mathbf{y}_3(t)=(0,0,0)$. A polar plot is shown of $r=|\mathbf{y}_1|=|\mathbf{y}_2|=\sqrt{r_1^2+r_2^2}$ vs $\varphi(\cos\varphi=\mathbf{y}_1\cdot\mathbf{y}_2/|\mathbf{y}_1|\cdot|\mathbf{y}_2|)$. Solution (c) belongs to (4.14). Solutions (b) and (c) have $\varphi=\pi/2$ just when both $\mathbf{y}_1$ and $\mathbf{y}_2$ reach the "equator": therefore their behavior on the "southern hemisphere" is the same as on the "northern hemisphere." Again, the trajectories are schematic.

with $r_2(t)\to 0$, $\alpha(t)\to 0$, $\beta(t)\to\beta_0$ for $t\to-\infty$. For each β_0 one finds two discrete sets of solutions with finite action, which accumulate on (4.6) (or some rotated analogue of it). For the first set both $\mathbf{y}_1$ and $\mathbf{y}_2$ pass simultaneously across the equator and $\mathbf{y}_1\cdot\mathbf{y}=0$ on the equator; the second set has somewhat more complicated symmetry properties on the equator. This then completes our discussion of trajectories of the following type. At the starting point both $\mathbf{y}_1$ and $\mathbf{y}_2$ point in the one-direction, and $\mathbf{y}_3=0$. Away from the starting point, $\mathbf{y}_1$ and $\mathbf{y}_2$ stay in the 1-2 plane and $\mathbf{y}_3$ remains zero. We have limited ourselves to those trajectories where the action integral is close to (4.8). By this we mean the following. There are, for example, other solutions in the vicinity of (4.6) and (4.7), which start from a toron point close to the origin, then for a long time oscillate around (4.6). Shortly before (4.6) reaches its end point, such a solution may turn back, again oscillates around (4.6), and finally ends on a toron point close to its starting point. Such a trajectory has approximately twice the action integral (4.8), and it is not counted as being "close to (4.8)." It is therefore clear that our search for solutions with finite action, even for this restricted class of initial conditions, is far from being complete.

We still have to go through few other solutions in the vicinity of (4.6). First we return to (4.9) and consider a more general spatial rotation. This leads to starting points of the form

$$Y_{\text{start}}=\begin{bmatrix} r_1 & & \\ & 0 & \\ & & 0 \end{bmatrix} R_{12}R_{13}R'_{12}=\begin{bmatrix} s_1 & s_2 & s_3 \\ 0 & 0 & 0 \\ 0 & 0 & 0 \end{bmatrix}. \tag{4.17}$$

(R_{ik} denotes a constant rotation in the ik plane). A computer analysis of the case $s_1=s_2\gg s_3$ shows that, as soon as s_3 differs from zero, the trajectory is pushed away from (4.6) and does not reach a toron point: for very small s_3 the trajectory for a long time follows (4.6), but shortly before (4.6) reaches its end point it deviates and turns back. Next we consider solutions which, in group space, no longer stay in the 1-2 plane. From Sec. III we know that a solution

$$Y=\begin{bmatrix} r_1 & & \\ & r_2 & \\ & & r_3 \end{bmatrix} \tag{4.18}$$

with $r_2(t)$, $r_3(t)\to 0$ for $t\to-\infty$ is attracted by the path (4.3): if r_3 initially is small, it follows for some time the solution (4.9) which in turn oscillates around (4.6). After a while, however, r_3 starts to grow, and before (4.9) reaches a toron end point, the trajectory escapes. We therefore conclude that, outside of the form (4.16), there are no solutions with finite action in the vicinity of (4.6)–(4.8).

We finally illustrate our results in the toron cube of Fig. 3. To this end we have to rotate (in group space) all our solutions: starting points of $\mathbf{y}_1$, $\mathbf{y}_2$, $\mathbf{y}_3$ have to point in the three-direction. Our main result then states that

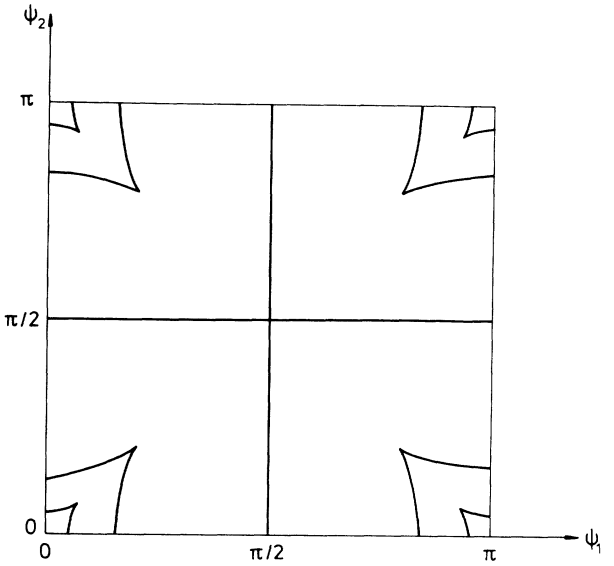

FIG. 9. The bottom of the toron cube of Fig. 2. The dark lines inside the square consist of starting points of solutions with finite action: in addition to the lines $\psi_1=\pi/2$, $\psi_2=\pi/2$ there are structures at the four corner points (approximately: squares). We have drawn only the largest ones, but there are more inside them, becoming smaller and smaller and finally accumulating at the corner points.

solutions with finite action [close to (4.8)] only start from toron points on the surface of the cube, not from the interior. For the bottom face of the cube we have illustrated, in Fig. 9, where solutions with finite action can start. (There are more lines closer to the corner points, but they are not visible on this scale.) As we have discussed in some detail, all these trajectories end on toron points, which also lie in the bottom plane, but near the corner point opposite to the starting point.

V. CONCLUSIONS

We first summarize the main results. This paper is part of a larger program which consists of a systematic study of the weak-coupling limit of lattice gauge theories. We make use of the Hamiltonian formulation and apply the semiclassical approximation. We are primarily interested in caustics, since the prefactor in the ground-state wave function which represents the quantum fluctuations around classical solutions becomes large and, hence, may provide significant contributions to physical quantities. Of particular interest are caustics in those regions of configuration space where the (exponentially decreasing) wave functions is not yet too small: this are field configurations close to the origin or other points with vanishing potential (=magnetic energy).

The first part of a semiclassical analysis consists of a detailed study of classical trajectories. In this paper we have begun to investigate a N^3 lattice model of pure SU(2) gauge theory, imposing periodic boundary conditions. We have found it convenient to first study only trajectories in the space of constant fields (momentum $\mathbf{k}=0$): putting $A_{\mathbf{k}}=0$ for all $\mathbf{k}\neq 0$, the classical equations

of motion reduce to a set of nine coupled equations which, by symmetry arguments, can be reduced further down to six or even three equations. It is the analysis of these equations of motion which we have presented in this paper.

Our results clearly demonstrate that, even in this restricted subspace of fields, classical trajectories exhibit a very rich structure, which includes the origin. In particular, caustics start right at the origin, and they consists of infinitely many nested cones with a cross section shown in Fig. 1. Both the existence and location of these caustics support the idea that we are pursuing: we are searching for regions close to the origin where caustics are dense, as candidates for a strong enhancement of the ground state wave function. We strongly expect that what we see in the $\mathbf{k}=0$ subspace is only a small part of a much larger structure. Results of this paper are therefore mainly viewed as an entry point into the complicated system of caustics. It may, however, also be that our analysis already contains some physics. We have seen that caustics are particularly dense near the field configurations $\{\mathbf{y}_1,\mathbf{y}_2,\mathbf{y}_3 \mid \mathbf{y}_1\cdot\mathbf{y}_2=\mathbf{y}_1\cdot\mathbf{y}_3=\mathbf{y}_2\cdot\mathbf{y}_3=0,\ \mathbf{y}_1^2=\mathbf{y}_2^2=\mathbf{y}_3^2\}$, i.e., all x links in the one-direction, all y links in the two-direction, and all z links in the three-direction. It therefore seems as if these "hedgehog" configurations may be of particular importance. As to the technical aspects of our analysis, we have shown that almost all relevant information (as far as the caustics are concerned) is contained in two unknown functions: f_1 and f_2, as defined in Sec. III. A qualitative analysis of these functions can be done by analytic methods; it is only for the numerical values of some parameters where the computer has been used.

We conclude with a few words about future steps. Clearly the next task will be the extension of our analysis to fields with $\mathbf{k}\neq 0$. We need to know how the caustics evolve when leaving the $\mathbf{k}=0$ subspace. In the previous section we have already obtained some indicates that, when both $\mathbf{k}=0$ and $\mathbf{k}\neq 0$ fields are taken into account, new caustics appear which start at some finite (but small) distance away from the origin. This will be confirmed in a forthcoming paper where we shall present a more detailed analysis of trajectories outside of (but close to) the $\mathbf{k}=0$ subspace: at distances of order $1/N$ trajectories of different momenta $\mathbf{k}$ start to intersect. This could be the beginning of the formation of caustics which belong to localized field configurations, i.e., fields which are concentrated around some site 1 on the lattice.

ACKNOWLEDGMENTS

Part of this work has been done while both of us where visitors at the CERN Theory Division. We wish to thank both M. Jacob and J. Ellis for making these visits possible and for their kind hospitality. The work of T. T. W. was supported in part by the U.S. Department of Energy under Grant No. DE-FG-02-84ER-40158.

[1]J. Bartels and T. T. Wu, Z. Phys. C **33**, 583 (1987).
[2]J. Kogut and L. Susskind, Phys. Rev. D **11**, 395 (1975).
[3]For constant fields the equations of motion are nonintegrable: see Refs. 8, 15, 19, and 21.
[4]For a recent review see M. Berry, in *Semiclassical Mechanics of Regular and Irregular Motion,* proceedings of Les Houches Lectures, Session XXXVI, 1981, edited by G. Iooss, R. H. G. Hellemann, and R. Stora (North-Holland, Amsterdam, 1983).
[5]V. A. Arnold, *Mathematical Methods in Classical Mechanics* (Springer, Berlin, 1987), Appendix 12.
[6]F. Wolf and H. J. Korsch, J. Chem. Phys. **81**, 3127 (1984), and references therein.
[7]M. Lüscher, Phys. Lett. **118B**, 391 (1982); Nucl. Phys. **B219**, 233 (1983).
[8]M. Lüscher and G. Münster, Nucl. Phys. **B232**, 445 (1984).
[9]P. van Baal, Nucl. Phys. **B264**, 548 (1986).
[10]J. Koller and P. van Baal, Nucl. Phys. **B273**, 387 (1986).
[11]A. Gonzales-Arroyo, J. Jurkiewicz, and C. P. Korthals-Altes, in *Proceedings of the Freiburg Summer Institute, 1981* (Plenum, New York, 1983), p. 339.
[12]B. Simon, Ann. Phys. (N.Y.) **146**, 209 (1983).
[13]H. M. Asatryan and G. K. Savvidy, Phys. Lett. **99A**, 290 (1983).
[14]G. Z. Baseynan, S. G. Matinyan, and G. K. Savvidy, Pis'ma Zh. Eksp. Teor. Fiz. **29**, 641 (1979) [JETP Lett. **29**, 587 (1980)].
[15]G. S. Matinyan, G. K. Savvidy, and N. G. Ter-Arutyunyan-Savvidy, Zh. Eksp. Teor. Fiz. **80**, 830 (1981) [Sov. Phys. JETP **53**, 421 (1981)].
[16]S. G. Matinyan, G. K. Savvidy, and N. G. Ter-Arutyunyan-Savvidy, Pis'ma Zh. Eksp. Teor. Fiz. **34**, 613 (1981) [JETP Lett. **34**, 590 (1981)].
[17]G. K. Savvidy, Phys. Lett. **130B**, 303 (1983).
[18]G. K. Savvidy, Nucl. Phys. **B246**, 302 (1984).
[19]E. S. Nikolaevskij and L. N. Shur, Pis'ma Zh. Eksp. Teor. Fiz. **36**, 176 (1982).
[20]G. K. Savvidy, Phys. Lett. **159B**, 325 (1985).
[21]B. V. Chirikov and D. L. Shepelyanskij, Pis'ma Zh. Eksp. Teor. Fiz. **34**, 171 (1981) [JETP Lett. **34**, 163 (1981)].

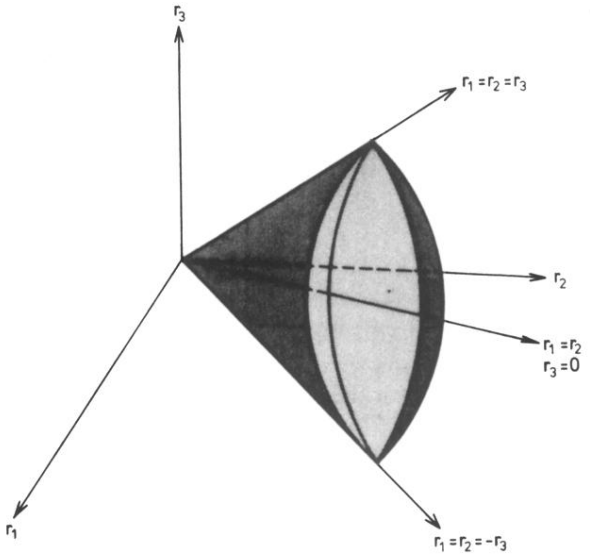

FIG. 1. Caustics in the vicinity of the origin. r_1, r_2, r_3 denote the three variables of the reduced Hamiltonian (3.9).